

2.8 μm Er:ZBLAN 光纤孤子自压缩放大器

周亦诚^{1,2}, 覃治鹏^{1,2*}, 谢国强^{1,2**}

¹ 上海交通大学物理与天文学院激光等离子体教育部重点实验室, 上海 200240;

² 上海交通大学 IFSA 协同创新中心, 上海 200240

摘要 理论和实验研究了一种 2.8 μm Er:ZBLAN 光纤孤子自压缩放大器。放大器采用锁模 Er:ZBLAN 光纤振荡器作为种子源, 锁模脉冲宽度为 240 fs, 峰值功率为 16.9 kW, 重复频率为 54.3 MHz。通过单级孤子自压缩放大, 实验获得了脉冲宽度为 110 fs、峰值功率达 151 kW 的中红外飞秒脉冲输出。

关键词 激光器; 超快激光器; 锁模激光器; 激光放大器; 红外和远红外激光器

中图分类号 TN248.1

文献标志码 A

doi: 10.3788/CJL202249.0101009

1 引言

中红外(波长为 2~20 μm)激光在分子光谱学、材料加工、生物医疗、基础物理研究等方面有着良好的应用前景^[1-6], 例如: 中红外波段拥有许多气体分子的特征吸收峰, 因此中红外激光可以应用于痕量气体探测^[7]; 聚焦的中红外激光能够深入到红外半导体材料的内部, 触发双光子/多光子吸收, 实现半导体材料的内部刻蚀^[8]。高峰值功率中红外超快激光还可以作为基础光源, 通过非线性频率变换(比如孤子自频移、参量下转换、超连续产生、带内差频等)产生光谱更宽、波长更长的中红外相干激光^[9-12]。

产生中红外超快激光的途径一般包括: 锁模全固态激光器、光参量振荡器/放大器以及锁模光纤激光器^[13-17]。其中, 光纤激光器兼具结构灵活、散热快以及光束质量好的特点, 是产生中红外超快激光的优良平台。目前的报道中常用 Er:ZBLAN 光纤作为增益介质来产生 2.8 μm 激光, 主要是因为 Er:ZBLAN 光纤可以采用高功率的 976 nm 半导体激光器泵浦, 并且交叉弛豫还能够突破量子亏损的限制^[18-19]。基于非线性偏振旋转锁模技术, 拉瓦尔大学的研究人员率先在 2.8 μm 波段实现了飞秒锁

模脉冲输出, 脉冲宽度为 207 fs、峰值功率为 3.5 kW^[20]。然而, ZBLAN 光纤在 2.8 μm 存在较大的负色散, 加上单模光纤具有较强的非线性, 导致腔内的孤子在较低峰值功率时就会分裂^[21]。为了获得更高的脉冲能量和峰值功率, 可对锁模脉冲进行放大^[22]。

本文报道了一种能够实现孤子自压缩的 2.8 μm Er:ZBLAN 光纤放大器。通过数值仿真, 分析了光纤增益、色散、自相位调制、拉曼效应对放大脉冲宽度和光谱的影响。放大器采用锁模 Er:ZBLAN 光纤振荡器作为种子源, 锁模脉冲的宽度为 240 fs、峰值功率为 16.9 kW。在无色散管理的情况下, 实验获得了脉冲宽度为 110 fs、峰值功率为 151 kW 的放大脉冲。在孤子自压缩的同时, 拉曼效应导致放大脉冲的光谱发生轻微的孤子自频移。

2 数值仿真

当脉冲宽度小于 1 ps 的超短脉冲在光纤中传输放大时, 除了要考虑增益、色散和自相位调制效应, 还需要考虑非线性拉曼效应。本研究采用广义非线性薛定谔方程对脉冲放大的演化过程进行模拟, 方程的具体表达式为^[23]

收稿日期: 2021-08-27; 修回日期: 2021-09-28; 录用日期: 2021-10-08

基金项目: 国家自然科学基金(62075126, 62005161, 91850203)、上海市“晨光计划”(19CG12)

通信作者: *lorance1205@sjtu.edu.cn; **xieqq@sjtu.edu.cn

$$\frac{\partial A(z, \tau)}{\partial z} - \frac{g}{2} A(z, \tau) - \sum_{n=2}^3 \frac{i^{n+1} \beta_n}{n!} \frac{\partial^n A(z, \tau)}{\partial \tau^n} = i\gamma A(z, \tau) \int_0^\infty R(\tau') |A(\tau - \tau')|^2 d\tau', \quad (1)$$

式中: $A(z, \tau)$ 为脉冲电场的慢变包络时域函数, τ 和 z 分别为延迟时间参数和传输坐标; g 为与频率相关的饱和增益函数,其小信号增益系数为 8 m^{-1} ^[24]; β_n 为ZBLAN光纤的各阶色散值; $\gamma = n_2 \omega_0 / c A_{\text{eff}}$ 为光纤的非线性系数, n_2 为克尔系数, ω_0 为载波频率, c 为光速, A_{eff} 为有效模场面积; $R(t) = (1 - f_R)\delta(t) + f_R h_R(t)$ 为ZBLAN光纤在中心波长附近的非线性响应函数,其中拉曼相应函数 $h_R(t) = (\tau_1^{-2} + \tau_2^{-2})\tau_1 \exp(-t/\tau_2) \sin(t/\tau_1)$, f_R 取值0.3, τ_1 、 τ_2 分别取值为16.7 fs和20.3 fs^[25]。

根据ZBLAN光纤的色散关系和几何参数,计算得到光纤的二阶色散 β_2 、三阶色散 β_3 、非线性系数 γ 分别为 $-84 \text{ fs}^2/\text{mm}$ 、 $500 \text{ fs}^3/\text{mm}$ 、 $1.66 \times 10^{-4} (\text{W} \cdot \text{m})^{-1}$ ^[26-27]。根据实验情况,输入信号设为傅里叶变换极限的sech型脉冲,宽度为240 fs,峰值功率为3.1 kW,放大器增益光纤长度为1.8 m。

图1(a)和图1(b)所示为不同增益下脉冲演化的模拟结果。当增益较低时,放大脉冲的峰值功率没有增大,脉冲宽度反而受到光纤自身色散的影响被展宽到904 fs,输出脉冲能量 E_{out} 被放大到4 nJ。

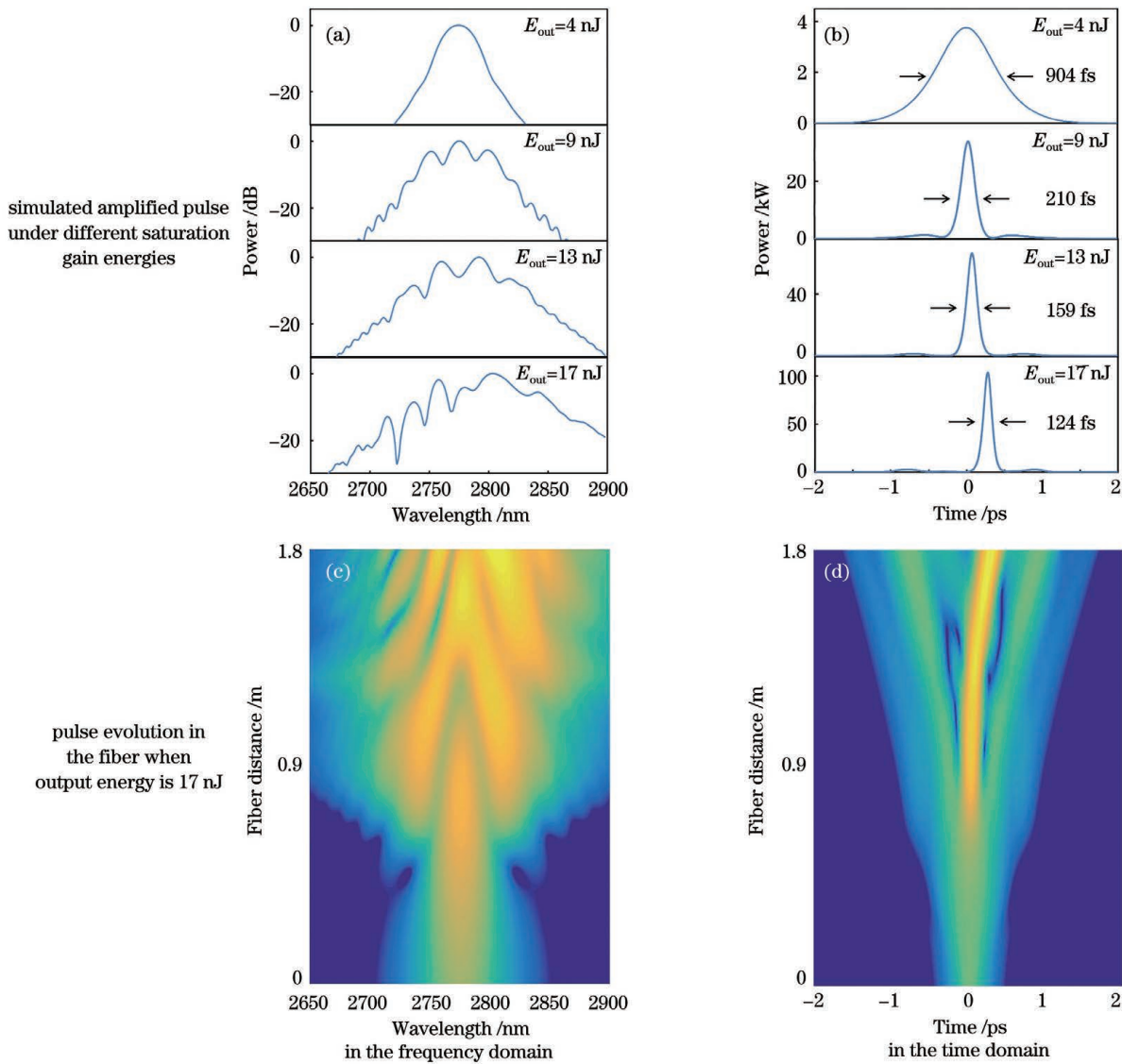


图1 不同增益时放大脉冲模拟结果以及输出能量为17 nJ时,脉冲在光纤内传播的演化过程

Fig. 1 Simulated amplified pulse under different saturation gain energies and pulse evolution in the fiber when output energy is 17 nJ

随着增益的提升,自相位调制能够抵消光纤反常色散的影响,放大脉冲宽度与种子脉冲宽度基本相当。当增益进一步提升,输出脉冲能量达到了 13 nJ,此时模拟输出脉冲宽度被压缩到 159 fs,并且放大光谱出现明显的展宽。当输出脉冲能量达到 17 nJ 时,模拟得到的脉冲宽度为 124 fs,此时脉冲光谱表现出红移迹象,并且短波部分的振荡更加剧烈,这是因为高峰值功率的脉冲在反常色散介质中发生孤子自频移。如果进一步提升增益,孤子自频移变得更加明显,脉冲开始分裂,不利于 2.8 μm 波段的孤子自压缩和峰值功率提升。

图 1(c) 和图 1(d) 所示分别为输出脉冲能量为 17 nJ 时脉冲信号沿光纤传播中在频率域和时间域的演化过程。借助这一演化过程,可以更直观地理解孤子自压缩的形成。首先,输入脉冲的峰值功率较低,不足以支持孤子传输。随后光纤的反常色散展宽了脉冲宽度,进一步限制了峰值功率的提升以及非线性相移的累积。随着脉冲在光纤中逐渐被放大,自相位调制开始发挥作用,脉冲前沿的频率成分发生红移,脉冲后沿的频率成分发生蓝移。由于较长波长的分量在反常色散介质中的群速度慢于较短波长的分量,频率受到调制后,前、后沿脉冲分量都往脉冲的时域中心聚集,使得脉冲最终呈现自压缩的效果。脉冲信号在光纤中传播时,初始位置的峰值功率较低,积累的非线性相移小,只在光纤后半段呈现较高的峰值功率,因此脉冲没有足够的传播距离来产生脉冲分裂。从模拟结果可以观察到,输出脉冲没有分裂。然而,放大脉冲在靠近输出端的高

峰值功率已经触发了拉曼效应,放大光谱通过孤子自频移出现了轻微的红移,如图 1(c) 所示。

3 实验装置

图 2 为 2.8 μm Er:ZBLAN 光纤放大器系统示意图,系统由锁模振荡器和放大器两部分组成。锁模振荡器采用物质的量分数为 7% 的 Er:ZBLAN(即 7% Er:ZBLAN)光纤(Le Verre Fluoré)作为增益介质,长度为 3 m。增益光纤的纤芯直径为 15 μm, 数值孔径 (NA) 为 0.12; 包层直径为 260 μm, 被间隔 240 μm 的两个平面所截,包层的 NA 为 0.46。光纤的两端以 8°角切割,以防止菲涅耳反馈形成寄生腔,干扰锁模运转。泵浦源为 976 nm 半导体激光器,通过 NA 为 0.22 的 105/130 多模光纤耦合输出,最高输出功率为 30 W。泵浦光经过 L₁(f₁=10 mm) 和 L₂(f₂=12.7 mm) 的透镜组准直和聚焦后,耦合进入锁模振荡器的增益光纤。通过截断法测量得到的耦合效率为 89%。其中,L₁ 透镜为石英透镜,L₂ 透镜为 ZnSe 非球面透镜并且镀有 2.8 μm (T>99.5%) 和 796 nm (T>95%) 的增透膜。在两镜之间,以 45°角放置一块 2.8 μm 高反(R>99.5%)、976 nm 高透(T>90%) 的合束镜。谐振腔整体为环形腔结构,在输出端放置透过率为 40% 的输出耦合镜。将半波片、1/4 波片和隔离器(Thorlab)组合起来,用于启动和维持非线性偏振旋转锁模。此外,隔离器的传输方向与泵浦光方向相同(即顺时针方向),有利于降低锁模阈值。

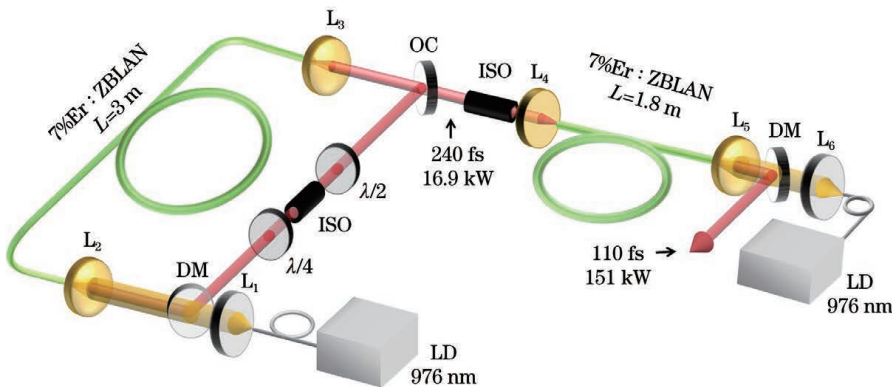


图 2 2.8 μm 锁模 Er:ZBLAN 光纤振荡器及放大器示意图

Fig. 2 Schematic of 2.8 μm mode-locked Er:ZBLAN fiber oscillator and amplifier

放大器采用相同的 Er:ZBLAN 光纤作为增益介质,光纤长度为 1.8 m。两端以 8°角切割,一方面是防止菲涅耳反射对锁模振荡器造成干扰,另一方面是为了提高放大器自发辐射放大的阈值。振荡器

和放大器之间的隔离器,能够阻断放大器的激光和泵浦光对振荡器的干扰,提高锁模振荡器的稳定性。放大器采用相向泵浦方式,有利于提高放大器的能量转换效率。

利用光电探测器(VIGO System, PCI-2TE-12)采集锁模脉冲,然后将其输入示波器和频谱分析仪进行锁模稳定性分析。示波器与频谱分析仪集成在一起,其型号为Tektronix公司的MDO3102型,工作带宽为1 GHz。使用热敏功率计(Thorlabs PM100D/S310C)测量输出功率,使用中红外自相关仪(APE,PulseCheck 150)和光谱仪(Ocean Optics,SIR5000)分别测量振荡器和放大器的输出脉冲宽度和光谱。

4 结果和分析

图3展示了振荡器输出脉冲的各项参数。当泵浦功率为1.5 W时,锁模运转较为稳定且能够自启动,振荡器的平均输出功率为220 mW。脉冲在纳秒和毫秒时间尺度内都能够保持强度一致性,如

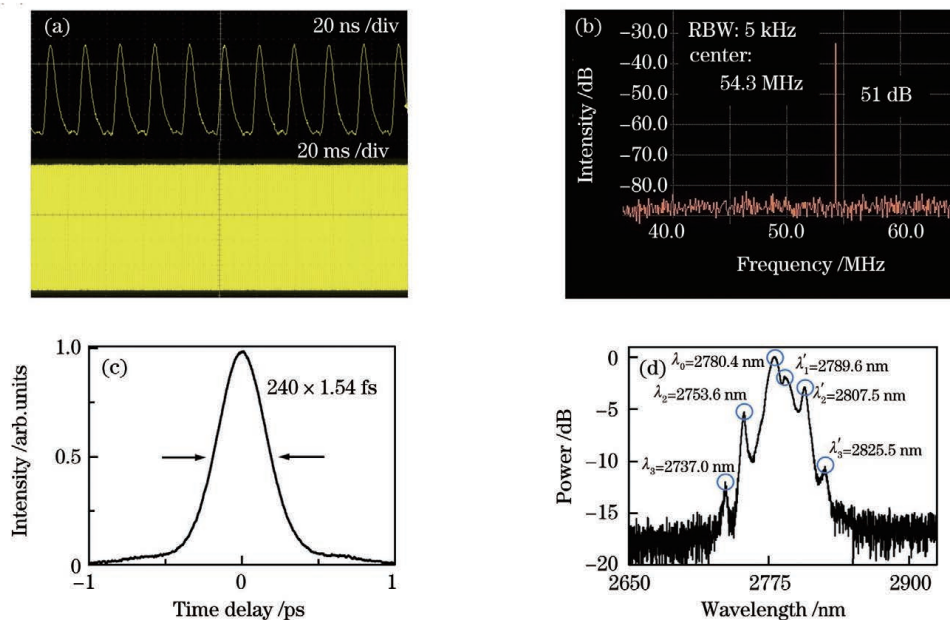


图3 锁模振荡器的输出结果。(a)纳秒和毫秒尺度的脉冲序列;(b)脉冲信噪比;(c)锁模脉冲自相关曲线;(d)锁模光谱

Fig. 3 Output performance of mode-locked oscillator. (a) Pulse train in nanosecond and millisecond time scales; (b) signal-to-noise ratio; (c) autocorrelation curve of mode-locked pulses; (d) mode-locked spectrum

放大器泵浦功率与输出功率的关系如图4所示。椭圆偏振种子光经过偏振相关的隔离器和光纤耦合后,平均输出功率降低到41 mW,相应的峰值功率为3.1 kW。当泵浦功率较低时,输出脉冲被展宽到皮秒水平,同时还出现增益窄化效应。受限于自相关的灵敏度,无法测量低峰值功率脉冲的宽度。当泵浦功率为3.75 W时,测量得到的放大脉冲宽度为247 fs。随着泵浦功率的增加,能够得到的最短脉冲宽度为110 fs,如图5(a)所示。此时的平均

图3(a)所示。通过进一步的频谱分析,可以得到脉冲序列的信噪比为51 dB,重复频率为54.3 MHz,如图3(b)所示。由此可得,振荡器输出的单脉冲能量为4.0 nJ。图3(c)所示为测量得到的强度自相关曲线,假定脉冲具有sech型轮廓,则锁模脉冲的半峰全宽为240 fs,对应的峰值功率为16.9 kW。图3(d)展示了测量得到的锁模光谱,可以清晰地观察到Kelly边带,这是孤子锁模的典型特征。各阶Kelly边带的位置和中心波长满足关系式: $\lambda_0 = 2\lambda_m \lambda'_m / (\lambda_m + \lambda'_m)$ ^[28],其中 λ_0 为中心波长, λ_m 为第m阶Kelly边带的短波波长, λ'_m 为第m阶Kelly边带的长波波长。受到水汽吸收的影响,第一阶Kelly边带的短波位置 λ_1 无法直观显示,通过计算得到 $\lambda_1 = 2771.2$ nm,其他各阶Kelly边带的位置如图3(d)所示。

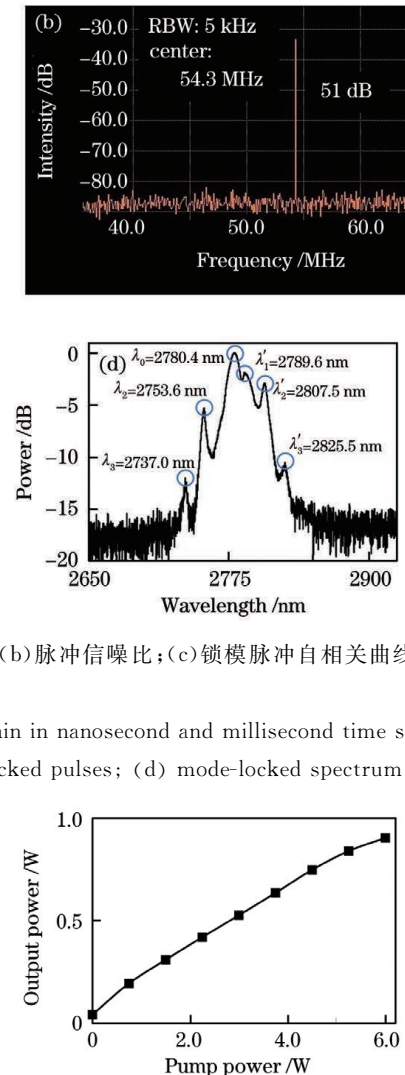


图4 放大器输出的平均功率和泵浦功率的关系

Fig. 4 Curve of amplifier output power with pump power

输出功率为 902 mW, 计算得到的单脉冲能量为 16.6 nJ, 峰值功率为 151 kW。相比于过去报道^[29]的无光栅的 2.8 μm Er:ZBLAN 光纤激光器的结果——峰值功率为 150 kW, 脉冲宽度约为 200 fs, 本实验的输出脉冲宽度缩短了一半。继续增大泵浦功率, 脉冲开始出现分裂。图 5(b)所示为 110 fs 放

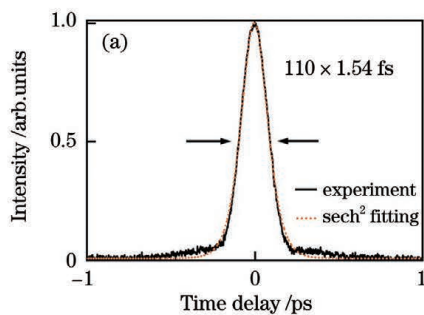


图 5 放大器输出结果。(a) 放大脉冲自相关曲线;(b) 放大光谱

Fig. 5 Output performance of amplifier. (a) Autocorrelation curve of amplified pulse; (b) amplified spectrum

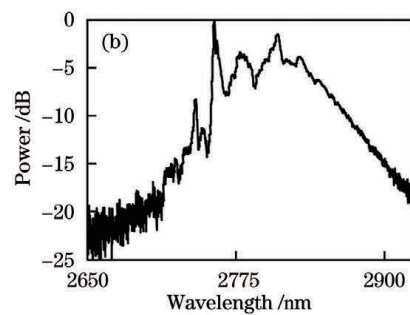
5 结论

研制了 2.8 μm Er:ZBLAN 光纤锁模振荡-功率放大系统。在振荡器部分, 采用非线性偏振旋转锁模技术获得了脉冲宽度为 240 fs 的孤子锁模脉冲输出。通过孤子自压缩放大, 实验获得了脉冲宽度为 110 fs、峰值功率为 151 kW 的 2.8 μm 中红外超短脉冲。结合理论与模拟分析, 证实了孤子自压缩放大是一种可靠的中红外超短脉冲激光产生方法。未来通过更进一步的色散管理与系统优化, 有望实现更高峰值功率的放大脉冲产生。

参考文献

- [1] Gattass R R, Mazur E. Femtosecond laser micromachining in transparent materials[J]. Nature Photonics, 2008, 2(4): 219-225.
- [2] Ebrahim-Zadeh M, Helmy A S, Leo G, et al. Mid-infrared coherent sources and applications: introduction[J]. Journal of the Optical Society of America B, 2021, 38(8): MIC1.
- [3] Mandon J, Guelachvili G, Picqué N. Fourier transform spectroscopy with a laser frequency comb [J]. Nature Photonics, 2009, 3(2): 99-102.
- [4] Archipovaite G M, Petit S, Delagnes J C, et al. 100 kHz Yb-fiber laser pumped 3 μm optical parametric amplifier for probing solid-state systems in the strong field regime[J]. Optics Letters, 2017, 42(5): 891-894.
- [5] Ma J, Qin Z P, Xie G Q, et al. Review of mid-infrared mode-locked laser sources in the 2.0 μm-
- [6] Liu J, Tan F Z, Liu C, et al. Progress on high-power ultrashort-pulsed thulium-doped fiber lasers[J]. Chinese Journal of Lasers, 2017, 44(2): 0201003. 刘江, 谭方舟, 刘晨, 等. 高功率超短脉冲掺铥光纤激光器的研究进展[J]. 中国激光, 2017, 44(2): 0201003.
- [7] Dong M, Zheng C T, Miao S Z, et al. Development and measurements of a mid-infrared multi-gas sensor system for CO, CO₂ and CH₄ detection[J]. Sensors (Basel, Switzerland), 2017, 17(10): E2221.
- [8] Nejadmalayeri A H, Herman P R, Burghoff J, et al. Inscription of optical waveguides in crystalline silicon by mid-infrared femtosecond laser pulses[J]. Optics Letters, 2005, 30(9): 964-966.
- [9] Hudson D D, Antipov S, Li L Z, et al. Toward all-fiber supercontinuum spanning the mid-infrared[J]. Optica, 2017, 4(10): 1163-1166.
- [10] Jia Z X, Yao C F, Li Z R, et al. Progress on novel high power mid-infrared fiber laser materials and supercontinuum laser[J]. Chinese Journal of Lasers, 2019, 46(5): 0508006. 贾志旭, 姚传飞, 李真睿, 等. 新型高功率中红外光纤激光材料与超连续谱激光研究进展[J]. 中国激光, 2019, 46(5): 0508006.
- [11] Yang L Y, Zhang B, He X, et al. 20.6 W mid-infrared supercontinuum generation in ZBLAN fiber with spectrum of 1.9-4.3 μm[J]. Journal of Lightwave Technology, 2020, 38(18): 5122-5127.
- [12] Liu K, Liang H K, Li W K, et al. Microjoule sub-two-cycle mid-infrared intrapulse-DFG driven by

大脉冲宽度对应的光谱。可以看到, 自相位调制导致光谱宽度从 67 nm 加宽到 128 nm(-10 dB), 并且拉曼效应使得放大光谱的中心波长从 2780 nm 红移到 2809 nm。由于拉曼效应产生的光谱曲线比较光滑, 因此可以看到光谱的长波部分调制相对较弱, 与数值模拟结果一致。



- 3- μm OPCPA [J]. IEEE Photonics Technology Letters, 2019, 31(21): 1741-1744.
- [13] Pushkin A V, Migal E A, Tokita S, et al. Femtosecond graphene mode-locked Fe:ZnSe laser at 4.4 μm [J]. Optics Letters, 2020, 45(3): 738-741.
- [14] Krogen P, Suchowski H, Liang H K, et al. Generation and multi-octave shaping of mid-infrared intense single-cycle pulses [J]. Nature Photonics, 2017, 11(4): 222-226.
- [15] Nie H K, Ning J, Zhang B T, et al. Recent progress of optical-superlattice-based mid-infrared optical parametric oscillators [J]. Chinese Journal of Lasers, 2021, 48(5): 0501008.
聂鸿坤, 宁建, 张百涛, 等. 光学超晶格中红外光参量振荡器研究进展 [J]. 中国激光, 2021, 48(5): 0501008.
- [16] Hu M L, Wang J, Fan J T. Research progress on fiber laser pumped femtosecond optical parametric oscillators [J]. Chinese Journal of Lasers, 2021, 48(19): 1901001.
胡明列, 王珏, 范锦涛. 光纤激光器泵浦的飞秒光学参量振荡器研究进展 [J]. 中国激光, 2021, 48(19): 1901001.
- [17] Pupeza I, Sánchez D, Zhang J, et al. High-power sub-two-cycle mid-infrared pulses at 100 MHz repetition rate [J]. Nature Photonics, 2015, 9(11): 721-724.
- [18] Li J F, Jackson S D. Numerical modeling and optimization of diode pumped heavily-erbium-doped fluoride fiber lasers [J]. IEEE Journal of Quantum Electronics, 2012, 48(4): 454-464.
- [19] Faucher D, Bernier M, Androz G, et al. 20 W passively cooled single-mode all-fiber laser at 2.8 μm [J]. Optics Letters, 2011, 36(7): 1104-1106.
- [20] Duval S, Bernier M, Fortin V, et al. Femtosecond fiber lasers reach the mid-infrared [J]. Optica, 2015, 2(7): 623-636.
- [21] Huang J, Pang M, Jiang X, et al. Route from single-pulse to multi-pulse states in a mid-infrared soliton fiber laser [J]. Optics Express, 2019, 27(19): 26392-26404.
- [22] Huang J, Pang M, Jiang X, et al. Sub-two-cycle octave-spanning mid-infrared fiber laser [J]. Optica, 2020, 7(6): 574-579.
- [23] Agrawal G P. Nonlinear fiber optics [M]. San Francisco: Academic Press, 2013.
- [24] Duval S, Olivier M, Fortin V, et al. 23-kW peak power femtosecond pulses from a mode-locked fiber ring laser at 2.8 μm [J]. Proceeding of SPIE, 2016, 9728, 972802: 9-16.
- [25] Nagl N, Mak K F, Wang Q, et al. Efficient femtosecond mid-infrared generation based on a Cr: ZnS oscillator and step-index fluoride fibers [J]. Optics Letters, 2019, 44(10): 2390-2393.
- [26] Gan F X. Optical properties of fluoride glasses: a review [J]. Journal of Non-Crystalline Solids, 1995, 184: 9-20.
- [27] Agger C, Petersen C, Dupont S, et al. Supercontinuum generation in ZBLAN fibers: detailed comparison between measurement and simulation [J]. Journal of the Optical Society of America B, 2012, 29(4): 635-645.
- [28] Smith N J, Blow K J, Andonovic I. Sideband generation through perturbations to the average soliton model [J]. Journal of Lightwave Technology, 1992, 10(10): 1329-1333.
- [29] Duval S, Gauthier J C, Robichaud L R, et al. Watt-level fiber-based femtosecond laser source tunable from 2.8 to 3.6 μm [J]. Optics Letters, 2016, 41(22): 5294-5297.

2.8- μm Er:ZBLAN Fiber Soliton Self-Compression Amplifier

Zhou Yicheng^{1,2}, Qin Zhipeng^{1,2*}, Xie Guoqiang^{1,2**}

¹ School of Physics and Astronomy, Key Laboratory for Laser Plasmas (Ministry of Education), Shanghai Jiao Tong University, Shanghai 200240, China;

² Collaborative Innovation Center of IFSA (CICIFSA), Shanghai Jiao Tong University, Shanghai 200240, China

Abstract

Objective Mid-infrared (2–20 μm) laser has a broad prospect in the applications including molecule spectroscopy, material processing, biomedicine, and basic physics research. Mode-locked all-solid-state laser, optical parametric oscillator or amplifier, and mode-locked fiber laser are some general methods for generating mid-infrared ultrafast laser. In the generation of this laser, the mode-locked fiber laser stands out owing to its advantages of flexible

structure, fast heat dissipation, and good beam quality. Currently, diode-pumped Er:ZBLAN fiber has been widely investigated at $2.8 \mu\text{m}$ because of its high gain and efficiency. Researchers from Laval University have realized femtosecond mode-locked pulses at $2.8 \mu\text{m}$ using a nonlinear polarization rotation technique, with a pulse width of 207 fs and a peak power of 3.5 kW. However, owing to the high nonlinearity of single-mode fiber and the large anomalous dispersion of ZBLAN fiber at $2.8 \mu\text{m}$, the intracavity soliton tends to split at a low peak power. It is an efficient way to amplify the mode-locked pulses to obtain higher pulse energy and peak power. In this study, we reported a $2.8\text{-}\mu\text{m}$ Er:ZBLAN fiber soliton self-compression amplifier with a pulse width of 110 fs and a peak power of 151 kW.

Methods Based on a generalized nonlinear Schrödinger equation, we numerically simulated the pulse evolution in the fiber amplifier. Influence of the saturation energy on the output pulses was investigated. The pulse evolution process in the fiber was used to explain the soliton-self-compression phenomenon in detail (Fig. 1). Guided by the simulated results, we constructed a $2.8\text{-}\mu\text{m}$ Er:ZBLAN fiber amplifier, seeded by a nonlinear polarization rotation (NPR) mode-locked Er:ZBLAN fiber laser (Fig. 2). The amplified pulses were characterized using a mid-infrared spectrometer (Ocean Optics, SIR5000) and intensity autocorrelator (APE, PulseCheck 150) under different incident pump powers.

Results and Discussions Fig. 1 shows the numerical simulation results. The pulse width of the seed pulse is 240 fs, and the peak power is 3.1 kW. The spectrum gradually broadens as the amplified pulse energy increases from 4 nJ to 17 nJ owing to the self-phase modulation [Fig. 1(a)]. The amplified pulse is shortened to 124 fs because of the combined effect of the anomalous dispersion and self-phase modulation [Fig. 1(b)]. Slight spectrum red-shift is observed through the soliton self-frequency shift. The soliton splitting due to the excess accumulation of nonlinear phase shift limits the higher pulse energy. Figs. 1(c) and 1(d) show the pulse evolution with the fiber in the time and frequency domains, respectively; the soliton self-compression process is clearly visible. Fig. 3 shows the experimental results of the mode-locked fiber laser. At 54.3 MHz, stable mode-locked pulses with a pulse width of 240 fs and a peak power of 16.9 kW are obtained. The seed source is connected to the amplifier fiber, and the average power output is measured (Fig. 4). The shortest pulse width after fiber amplification is 110 fs [Fig. 5(a)]. The center wavelength is shifted from 2780 nm to 2809 nm [Fig. 5(b)]. When the pulse energy reaches 16.6 nJ, the calculated peak power of the output pulse is 151 kW. Pulse splitting is observed as the pump power increases further.

Conclusions Herein, we report a high-peak-power Er:ZBLAN fiber amplifier at $2.8 \mu\text{m}$ that is seeded by an NPR mode-locked Er:ZBLAN fiber laser with a pulse width of 240 fs and a peak power of 3.1 kW at 54.3 MHz. A numerical simulation of the model amplifier based on a generalized nonlinear Schrödinger equation is used to analyze its operation and demonstrate the soliton self-compression process. We experimentally obtain the amplified pulses with a pulse width of 110 fs and a peak power of 151 kW. Our results show that self-compression amplification is a reliable method for producing high-peak-power mid-infrared ultrashort pulses at $2.8 \mu\text{m}$. In future, higher-peak-power pulses are expected from the Er : ZBLAN fiber amplifier through dispersion management and system optimization.

Key words lasers; ultrafast lasers; mode-locked lasers; laser amplifiers; infrared and far-infrared lasers